Integrative Additive Design for Robust SEI Formation in NMC811||Silicon Batteries

Xianyang Wu,[a] Xinlin Li,[a] Zhenzhen Yang,[a] Brian J. Ingram,[a] Matthew Li,[a] Chi-Cheung Su,[a,*] and Khalil Amine [a,b]*

[a]Chemical Sciences and Engineering Division, Argonne National Laboratory, Lemont, Illinois 60439, United States
[b]Pritzker School of Molecular Engineering, University of Chicago, Chicago, IL 60637, United States

Corresponding authors: csu@anl.gov; amine@anl.gov

Abstract: Silicon (Si) is considered a promising replacement for graphite anodes in lithium-ion batteries (LIBs) due to its high abundance and exceptional specific capacity. However, its widespread commercialization has been hindered by poor electrochemical performance. Among various strategies, the use of functional additives has emerged as one of the most effective and cost-efficient methods to enhance the electrochemical properties of LIBs. In this study, several additives—vinylene carbonate (VC), vinyl ethylene carbonate (VEC), lithium difluorophosphate (LiDFP), lithium difluoro(oxalato)borate (LiDFOB), lithium tetrafluorooxalatophosphate (LiTFOxP), and lithium difluorobis(oxalato)phosphate (LiDFBOP)—were systematically investigated in $LiNi_{0.8}Mn_{0.1}Co_{0.1}O_2$ (NMC811)||Si full cells. Notably, LiDFBOP, a lithium salt containing two oxalate groups, outperformed all other additives, delivering the best capacity retention after 300 cycles. Comprehensive characterizations, including FTIR, SEM, and XPS, revealed that LiDFBOP's superior performance stems from its ability to form a more stable solid electrolyte interphase (SEI) on the Si anode, owing to its favorable molecular structure that integrates the beneficial features of the other additives.

TOC graphic

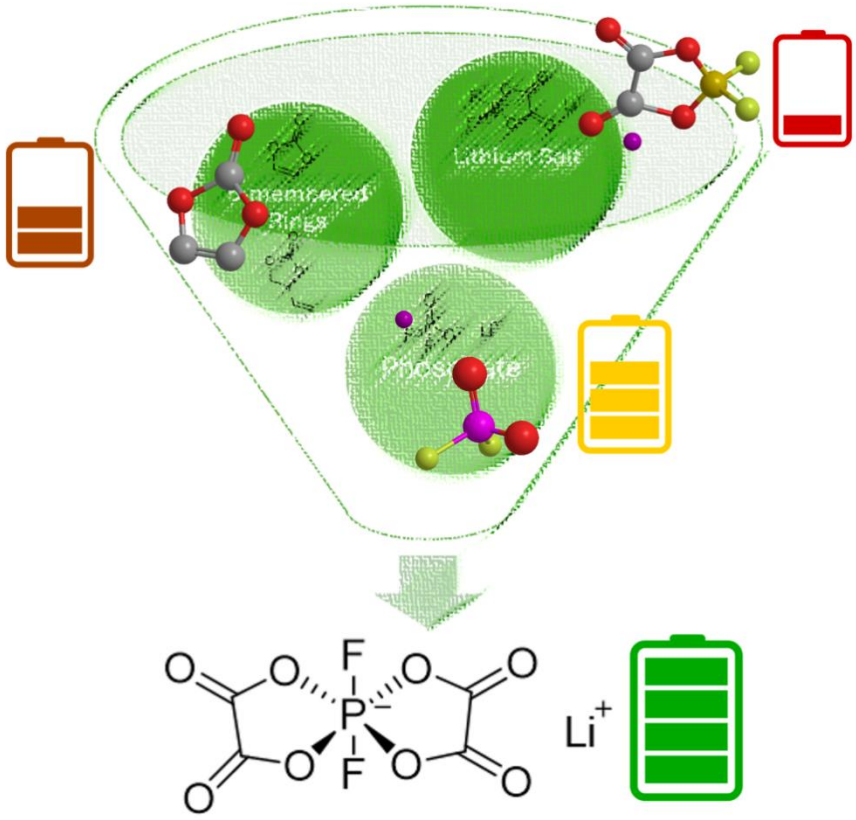

Introduction

The development of lithium-ion batteries (LIBs) with higher energy density has always attracted significant interest within the LIB community, and the utilization of electrode materials with higher specific capacities is a straightforward strategy.[1] Silicon (Si) anodes have long been considered a potential replacement for graphite in LIBs due to their significantly higher specific capacity (4000 mAh/g) compared to graphite (372 mAh/g) and their abundance, constituting 28.2% of the Earth's crust.[2,3] However, despite these advantages, Si still faces tremendous challenges as an electrode material. It suffers from intrinsically low electronic conductivity (~10^{-3} S/cm) and sluggish kinetics.[4,5] Moreover, during lithium alloying, Si experiences a large volume expansion (~300%) when transitioning from Si to $Li_{21}Si_5$, which leads to pulverization and loss of electrical contact.[6,7] This, in turn, causes the fracture of the solid electrolyte interphase (SEI) and continuous side reactions between the Si electrode and the liquid electrolyte, hindering commercialization.[8-10]

To address these challenges, various strategies have been explored to enhance the electrochemical performance of Si electrodes. For binders, the development of multifunctional binders with improved adhesion strength and ionic conductivity has garnered significant attention.[11-14] Additionally, efforts to mitigate side reactions between the Si electrode and the liquid electrolyte have led to the proposal of various electrolyte formulations, including solvents derived from carbonates,[15-17] esters,[18,19] ethers,[20,21] and sulfur-based compounds.[22-24] To accommodate the volume expansion during lithium alloying and prevent fractures, numerous structural modifications, such as nanostructured Si (e.g., nanotubes, nanowires, nanoparticles) and morphological designs (e.g., core-shell, yolk-shell, porous structures), have been investigated.[25-29]

Functional additives have long been recognized as one of the most effective and cost-efficient methods to improve the overall performance of LIBs.[30-37] A variety of additives, such as fluoroethylene carbonate (FEC), vinyl ethylene carbonate (VEC), vinylene carbonate (VC), and Lithium difluoro(oxalato)borate (LiDFOB), have been widely studied in Si-containing LIBs to enhance their long-term cycling performance. For example, Choi et al. studied FEC as an additive in thin-film Si anodes, finding significant improvements through the formation of stable compounds within the SEI.[38] Liao et al. investigated the effect of 1% VC additive on Si film electrodes, demonstrating that it retained over 50% of its initial capacity after 500 cycles due to the formation of an SEI that is impermeable to the liquid electrolyte.[39]

In this study, various electrolyte additives with distinctive chemical features—lithium difluorophosphate (LiDFP), lithium difluorobis(oxalato)phosphate (LiDFBOP), lithium tetrafluorooxalatophosphate (LiTFOxP), LiDFOB, VEC and VC—were systematically examined in NMC811||Si full cells. The baseline electrolyte consisted of 1.2 M $LiPF_6$ in a 3:7 mixture of ethylene carbonate (EC) and ethyl methyl carbonate (EMC) (Gen2), with 3 wt% FEC. Interestingly, the as-received LiDFBOP exhibits insufficient purity for battery applications and thus requires recrystallization to obtain a high-purity salt. The ^{31}P and ^{19}F NMR spectra of the purified LiDFBOP are shown in **Figures**

S1 and **S2**, respectively. Electrochemical testing revealed that the presence of both a cyclic oxalate and a phosphate group in the lithium salt additives contributed significantly to robust SEI formation on the Si anode. Among all additives, LiDFBOP demonstrated the highest capacity retention and average specific capacity (**Table S1**), attributed to its unique structure featuring two oxalate rings.

The design rationale behind LiDFBOP is summarized in **Scheme 1**, which highlights the beneficial structural motifs from each additive and their synergistic integration in LiDFBOP. The partial fluorination and the incorporation of multiple oxalate moieties on the anion structure is expected to tune the interphase composition on the Si anode. The evolution of the solvation structure was probed using Fourier-transform infrared (FTIR) spectroscopy. Post-cycling analysis of NMC811 cathodes in coin cells confirmed the preservation of the crystal structure, with performance degradation mainly due to irreversible loss of active lithium, not cathode degradation. First charge capacities of cycled NMC811||Li half cells were comparable across all additive systems, indicating that the observed differences in full-cell performance originated primarily from the Si anode. Scanning electron microscopy (SEM) showed that Si anodes cycled with LiDFBOP retained good adhesion to the Cu current collector after 300 cycles, while those with other additives exhibited delamination. X-ray diffraction (XRD) confirmed the structural integrity of NMC811 cathodes, with lattice parameter changes again pointing to lithium loss rather than structural collapse. Finally, X-ray photoelectron spectroscopy (XPS) revealed that the superior electrochemical performance of LiDFBOP stemmed from its ability to form a stable and protective SEI on the Si anode.

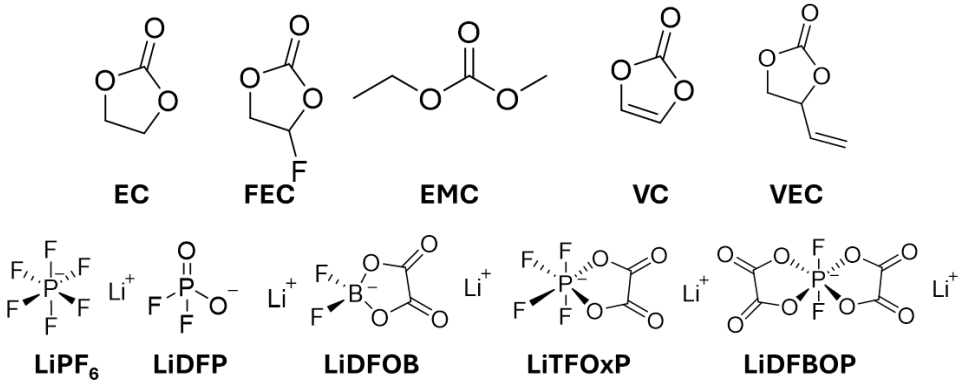

Figure 1. Chemical structures of all electrolyte components evaluated in this study.

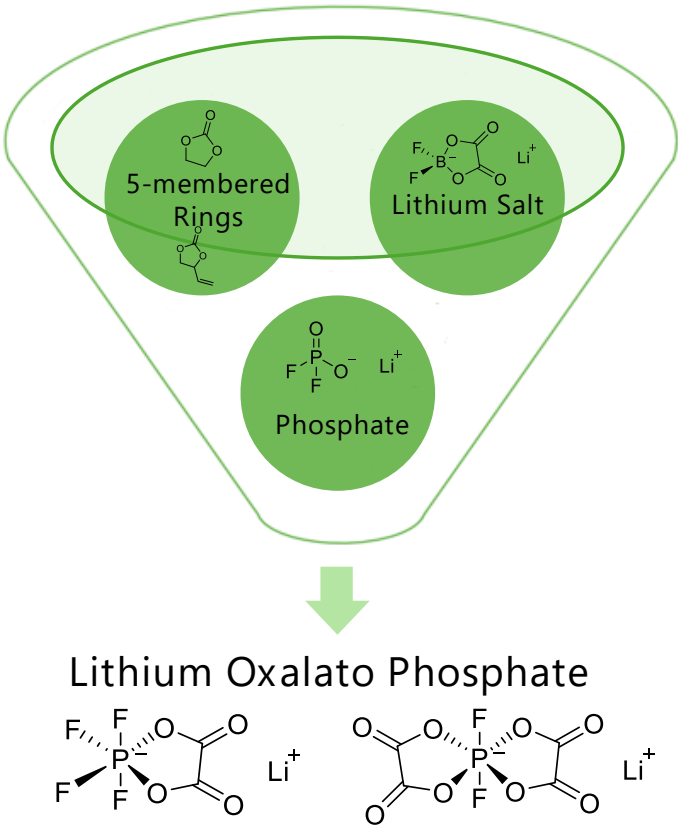

Scheme 1. The design rational behind various additives probed in this study.

Experimental Section

Preparation of liquid electrolytes: The Gen2 electrolyte, composed of 1.2 M $LiPF_6$ dissolved in a mixture of EC and EMC at a weight ratio of 3:7, was purchased from TOMIYAMA PURE CHEMICAL INDUSTRIES, LTD. Gen2 with 3 wt% FEC was selected as the baseline electrolyte. VC and VEC were obtained from Sigma-Aldrich, while FEC, LiDFP, LiDFOB, LiTFOxP, and LiDFBOP were sourced from MSE Supplies. FEC, VC, and VEC were dried over molecular sieves and further purified by vacuum distillation prior to use. LiDFP, LiDFOB, and LiTFOxP were used as received. LiDFBOP was purified by recrystallization with acetonitrile. The precipitated crystals were harvested by filtration. The ^{31}P and ^{19}F

NMR spectra of the purified LiDFBOP are displayed in **Figures S1** and **S2** respectively. The six additional electrolytes, each consisting of the baseline electrolyte with 2 wt% additive, were prepared inside an argon-filled glovebox with oxygen and moisture levels maintained below 1 ppm.

Electrochemical Testing: The electrodes were provided by Cell Analysis, Modeling, and Prototyping (CAMP) Facility at Argonne National Laboratory, and their detailed components were summarized in **Table 1**. The electrodes received were first dried in the vacuum chamber at 120 °C overnight before use. The separator is 17mm Celgard 2325. Before long-term cycling, all prepared coin cells (14 mm NMC811 and 15 mm Si) experienced a formation process before long-term cycling, with charging cutoff voltage increasing stepwisely from 4.12 V, 4.13 V, 4.15V, 4.17 V, 4.19 V and 4.2 V. 40 µL liquid electrolyte was used for each coin cell. For the long-term cycling experiments, the constant current charging/discharging protocol was used, and prepared coin cells were cycled on a Maccor tester, with voltage range between 3.0-4.2 V vs Li/Li^+ at C/3, with 1C capacity of 3.2 mAh. To prepare NMC811||Li half cells, cycled NMC811 cathodes taken out of cycled NMC811||Si full cells were first rinsed with pure EMC solvents and then they were vacuum dried in the anti-chamber of glovebox overnight. Then they were used for the preparation of NMC811||Li half cells. And 40 µL Gen2 electrolytes were used for all prepared NMC811||Li half cells. The prepared NMC811||Li half cells were then cycled between 2.5-4.3 V vs Li/Li^+ at C/20 with 1C capacity of 3.2 mAh. For the electrochemical impedance spectroscopy (EIS) experiment, it is implemented at BioLogic (VSP300) within the frequency range from 500 KHz to 0.1 Hz.

Table 1. Detailed compositions of NMC811 cathodes and Si anodes obtained from CAMP

	Cathode	**Si Anode**
Composition	NMC811	Si
Active material	90 wt% Targray NMC811	80 wt% Si
Binder	5 wt% Solvay 530 poly(vinylidene fluoride) (PVDF)	10wt% P84 Polyimide by Ensinger
Conducting agent	5 wt% Timcal C45 carbon	10 wt% Timcal C45 carbon
Loading density (mg/cm^2)	15.81	1.19
Coating thickness (µm)	59	14

Areal capacity (mAh/cm^2)	2.59	2.07
Porosity	34.5%	57.2%

Fourier-transform infrared (FTIR) spectroscopy: A PerkinElmer ATR Alpha FT-IR spectrometer, equipped with a diamond crystal as the refractive element was used to record the IR spectra. Measurements were conducted at 25 °C, covering a spectral range of 400–4000 cm^{-1} with a resolution of 2 cm^{-1}. Each sample spectrum was obtained using a single scan to avoid solvent evaporation.

Scanning electron microscope (SEM): All micrographs were collected on a JEOL IT800HL scanning electron microscope. Generally, with the accelerating voltages ranged between 10 and 20 kV and the pressure <10 e^{-4} mbar. All samples were first rinsed with battery grade DMC solvent to remove residual Li salts and dried in vacuum.

X-ray Diffraction (XRD): For the powder diffraction experiments, they were implemented on the Bruker D8 diffractor.

X-Ray Photoelectron Spectroscopy (XPS): For all the electrodes, they were rinsed with DMC 3 times and dried in the anti-chamber overnight. Further XPS was conducted on a Thermo Scientific NEXSA with a monochromatic Al Ka source and 200 μm spot size. All fitting was conducted on the Thermo Scientific Avantage software and data was referenced to the adventitious carbon C 1s peak at 284.8 eV. The Gaussian/Lorentzian ratio was the same for all peaks in each orbital. The full width half maximum was set to 1.7 eV and the same for all peaks in each orbital.

Results and discussion

Additive Effect on Electrochemical Performance: To evaluate the reduction behaviors of the additives, Li||Si half cells using the baseline electrolyte and electrolytes with various additives were first prepared and cycled between 0.05-2.5 V vs. Li/Li$^+$. The differential capacity (dQ/dV) profiles of all tested additives were thus obtained, and the results were summarized in **Figure S3**. The oxalato-phosphate salt

exhibits a higher reduction potential than the oxalato-borate salt, making it more likely to undergo preferential reduction and contribute to SEI formation. Moreover, the reduction potential increases with the number of oxalate groups in the molecule. Specifically, the LiDFOB additive is reduced at approximately 1.56 V vs. Li/Li^+, LiTFOxP at ~1.82 V, and LiDFBOP at ~1.97 V vs. Li/Li^+. No distinct reduction peak was observed in the cell containing LiDFP, indicating that the reduction potential of LiDFP is lower than that of FEC.

To assess their oxidative stability at elevated voltages, NMC811||Li half-cells were prepared and tested at 4.4 V and 4.5 V with a voltage hold time of 20 hours. This was done in reference to the 4.3 V cutoff voltage used for NMC811||Si full cells, and the results are shown in **Figure S4**. At 4.4 V, the static leakage currents of all half-cells—regardless of the electrolyte additive—are comparable to that of the baseline cell, indicating that both the additives and the baseline electrolyte are stable at this voltage versus Li/Li^+. However, at 4.5 V, the LiTFOxP-containing cell exhibits a significantly higher leakage current, pointing to electrolyte decomposition and an unstable cathode–electrolyte interphase. The LiDFOB-containing cell also shows an elevated leakage current compared to the other samples, suggesting a less stable interphase, though still more stable than that of LiTFOxP. In contrast, the remaining additive-containing samples show leakage currents similar to the baseline, indicating good interphase stability at 4.5 V.

After evaluating the reduction behavior and oxidation stability under increasing voltage, the long-term electrochemical performance within NMC811||Si full cells were subsequently tested. The 1^{st} cycle Coulombic efficiencies (CEs) and discharge specific capacity of all tested cells were depicted in **Table S1.** During the first cycle of the formation process, most electrolytes exhibit a CE of approximately 60%, with the LiTFOxP sample showing the lowest CE at about 49.7%. Given the high silicon content (80%) and the particle size of the Si anode, the low CE during the first cycle is typical. This low CE is primarily due to the significant volume expansion and the failure/fracture of the SEI formed on the Si anode.[40,41] Regarding the first discharge capacity during the formation process, most electrolytes show a specific

capacity of around 1500 mAh/g, while the LiTFOxP sample exhibits a lower specific capacity of approximately 1188 mAh/g and the LiDFBOP sample shows 1418 mAh/g.

A summary of the average CE, average capacity, and capacity retention over the first 200 cycles is provided in **Figure S5**. During the initial 10 cycles, all tested electrolytes exhibit increasing CE values, attributed to SEI formation and thickening on the Si electrodes. After 300 cycles, the LiDFBOP sample maintains the highest CE of 99.5% and a discharge-specific capacity of 532 mAh g^{-1}. The evolution of CE over cycling shows that, unlike other samples, the LiDFBOP cell maintains a consistently high CE. In contrast, the remaining cells follow a trend of initial stability, followed by a sharp decline and eventual gradual recovery. This behavior likely reflects the progressive consumption of the additive: initially, the presence of the additive supports stable CE; once depleted, CE declines; and the subsequent recovery may be due to reduced lithium alloying with Si. The stable CE observed in the LiDFBOP cell suggests the formation of a more robust and durable electrolyte–electrode interface. Besides, charge-discharge curves at selected cycles (shown in **Figure S6**) have been obtained and it is found that the baseline electrolyte exhibits higher overpotential than the other three electrolytes with additives.

The long-term cycling performance and CEs of the tested electrolytes in NMC811||Si full cells are shown in **Figure 2**. Among all formulations, the electrolyte containing LiDFBOP delivers the best overall performance. Most cells exhibit substantial capacity fade after approximately 100 cycles, and by 300 cycles, only the LiDFBOP and LiTFOxP cells retain appreciable capacity, whereas the others show near-complete loss. VC and VEC offer modest improvements over the baseline—likely due to their cyclic oxalate structures—but still fall short compared to the more effective additives. Interestingly, although the LiTFOxP cell starts with the lowest CE and discharge capacity, it maintains more stable long-term performance than the baseline, VC, VEC, LiDFP, and LiDFOB cells. The LiDFP cell also outperforms VC, VEC, and the baseline, highlighting the positive effect of lithium fluorophosphate. Similarly, the LiDFOB cell shows improved cycling stability, suggesting that incorporating a cyclic oxalate into the

lithium salt contributes to enhanced performance. Overall, LiDFBOP, which integrates multiple beneficial functional groups, enables the most robust battery performance among the tested additives.

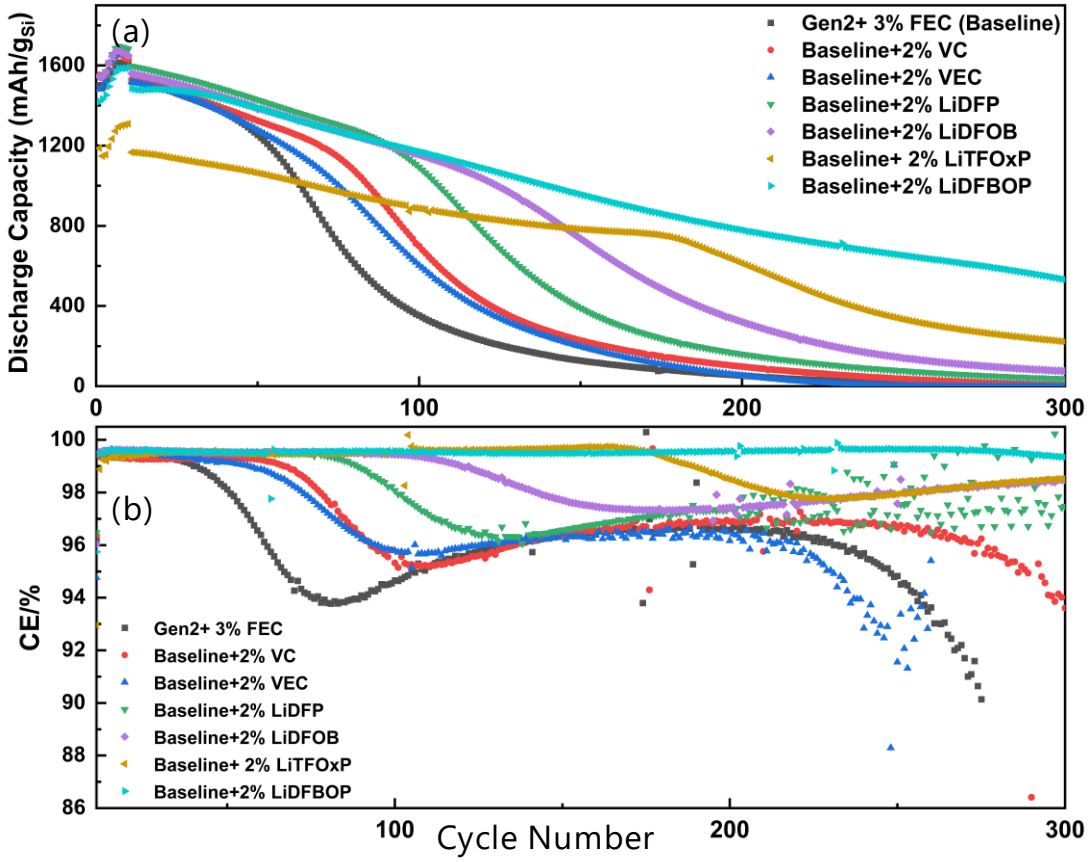

Figure 2. (a) The long-term cycling performance for tested electrolytes within NMC811||Si full cells; (b) corresponding CEs of tested electrolytes.

Solvation Structures of Electrolytes with Various Additives: To better understand the various long-term cycling performances of tested electrolyte samples, various characterizations further implemented. Given the crucial role of solvation structure in determining the interfacial chemistry at the Si anode, the evolution of the solvation structure for the tested electrolyte systems was examined using Fourier-transform infrared (FTIR) spectroscopy. The results are summarized in **Figure 3** and **Figures S7**. To qualitatively analyze the evolution of the solvation structures, FTIR spectra for $LiPF_6$ dissolved in pure EMC and a 3:7 wt% mixture of EC/EMC were obtained and were also shown in **Figures 3c** and **Figure 3d**, with the full FTIR spectra provided in **Figure S7**.

For EMC (**Figure S7a** and **Figure 3c**), the C=O vibration from the carbonyl group shifts from approximately 1744 cm^{-1} to 1710 cm^{-1} upon coordination with Li^+. As the concentration of $LiPF_6$ salt increases, the ratio of coordinated EMC also increases as the ratio of C=O bond at ~1710 cm^{-1} increases significantly. Similarly, for $LiPF_6$ solvated in the EC/EMC mixture (**Figure S7b** and **Figure 3d**), comparable trends are observed. In the absence of Li salts, the absorption peaks at approximately 1805 cm^{-1}, 1775 cm^{-1}, and 1744 cm^{-1} are attributed to the stretching vibration of uncoordinated carbonyl groups of EC, the Fermi resonance of carbonyl bands from EC, and the stretching vibration of uncoordinated carbonyl groups of EMC, respectively. Given the fact that EC has Fermi resonance, no further analysis was implemented on peaks from EC. After the addition of $LiPF_6$ salts, the solvation structure undergoes significant changes: as the concentration of $LiPF_6$ increases, the coordinated C=O bonds of EMC increase notably.

Based on the evolution of the EMC peaks (<1760 cm^{-1}), which are clearly distinguishable from the highly overlapping region (>1770 cm^{-1}) containing the peaks of FEC, EC, and the carbonyl absorption of oxalate, it is evident that the coordination ratio of EMC increases with the addition of lithium salt additives (**Figure 3b**). This trend is consistent with the expectation that additional lithium cations—similar to an increase in $LiPF_6$ concentration—promote greater coordination with EMC. However, the overall change in coordination ratio remains relatively small, likely due to the limited amount of additive (2 wt%) introduced, which is insufficient to significantly alter the bulk solvation structure of the electrolyte.

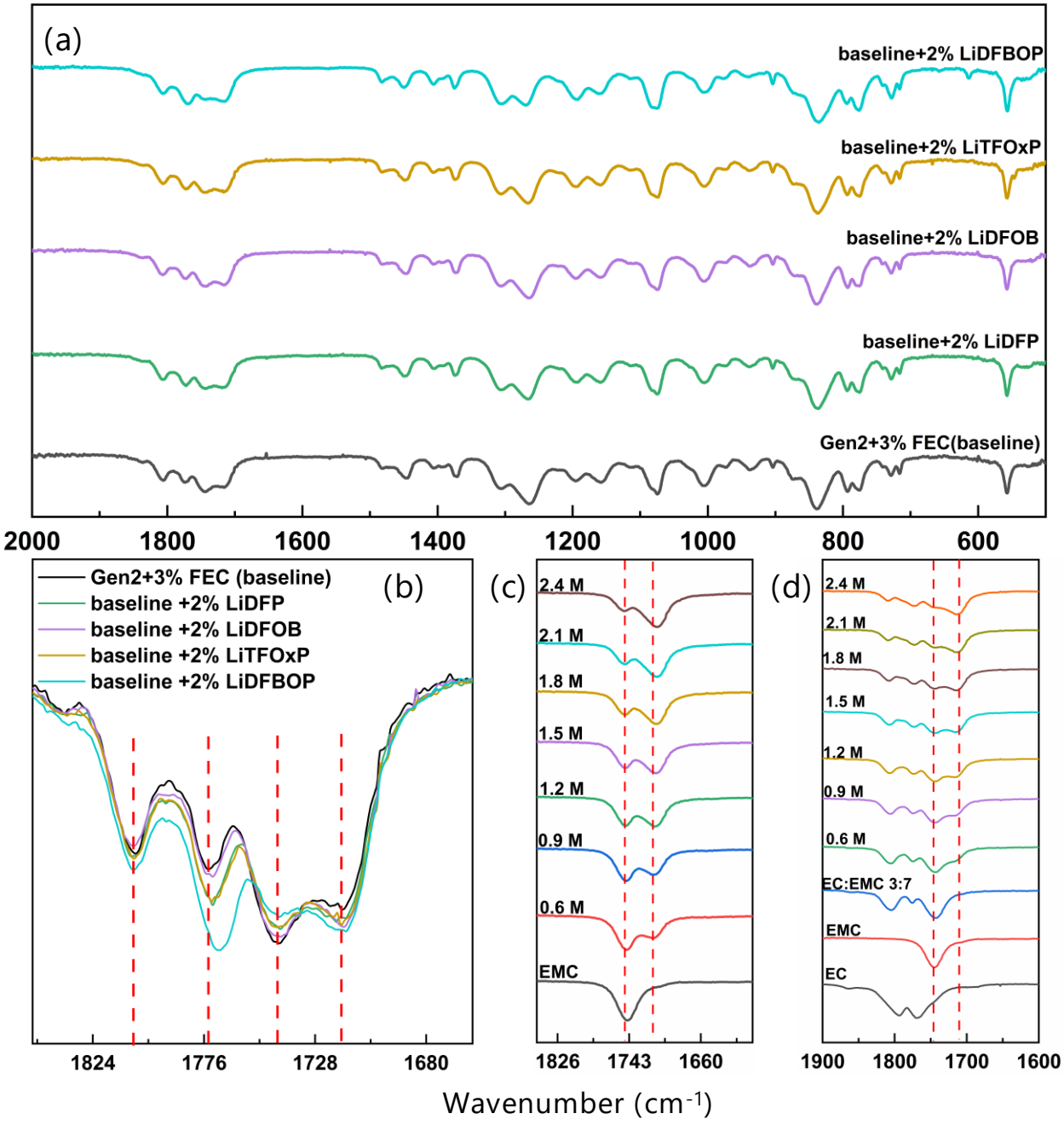

Figure 3. The FTIR spectra of tested electrolytes with various additives (a) the full spectra between 2000 cm^{-1} and 500 cm^{-1}; (b) the FTIR spectra between 1850 cm^{-1} and 1660 cm^{-1}; additives (c) the FTIR spectra of increasing $LiPF_6$ salt concentration solvated in pure EMC solvent, between 2000 cm^{-1} and 500 cm^{-1}; (d) the FTIR spectra of increasing $LiPF_6$ salt concentration solvated in EC/EMC solvents (with weight ratio of 3:7), between 2000 cm^{-1} and 500 cm^{-1}.

***Structural Evolution of NMC811 Cathode*:** To further identify the factor influencing the long-term cycling performance, cycled NMC811 cathodes were extracted from the coin cells to prepare NMC811||Li half cells. The voltage-specific capacity profiles of the first two cycles for the prepared NMC811||Li half cells are depicted in **Figure S8**.

From the first charge profile shown in **Figure S8a**, the active lithium content remaining within the NMC811 electrode (after 300 long-term cycles) can be determined. These electrodes consistently show higher specific capacity than the 300th discharge capacity in the NMC811||Si full cells, which clearly suggests that the Si anode determines the discharge capacity in the NMC811||Si full cells. It is also evident that, generally, better capacity retention in the NMC811||Si full cells correlates with a lower amount of active lithium remaining within the NMC811 electrode. This makes good sense, as more lithium is lost to the Si anodes during long-term cycling. Additionally, it was observed that the NMC811 electrode from the baseline electrolyte exhibit a voltage-capacity profile with a first decrease followed by an increase, whereas the other NMC811 electrodes do not show such an abnormal trend. This behavior is likely due to harmful decomposition residues left on the NMC811 electrode after long-term cycling, indicating more severe decomposition of the baseline electrolyte.

From the second voltage-capacity profile shown in **Figure S8b**, it is apparent that all electrodes exhibit a specific capacity greater than 125 mAh/g. This increased capacity is attributed to the active lithiums that were compensated by the lithium metal into the NMC811 electrodes during the first discharge process. It is also seen that the NMC811 electrode from the baseline electrolyte still exhibit the lowest charge-discharge capacity, even after lithiation after the 1st discharge. This is possibly due to increased internal resistance from harmful decomposition residues.[42]

This indicates similar contents of reversible Li^+ for NMC811 electrodes experiencing 300 cycles, suggesting the Si anodes are the major player in leading to the various performances to the NMC811||Si full cells. Meanwhile, for the rinsed NMC811 cathodes, their XRD results are summarized in **Figure 4**. Compared to the XRD pattern from pristine NMC811, cycled NMC811 cathodes exhibit the same XRD

patterns, indicating well maintenance of bulk crystal structure after long-term cycling. Compared to the pristine NMC811, it is seen that major peaks of cycled NMC811 electrodes are well maintained after 300 cycles. And there are significant peak shifting for 003 peaks for all cycled NMC811 electrodes, with the LiDFBOP sample exhibiting largest shift. This peak shift to lower positions reveals the increase of lattice parameter *c* of NMC811 and it is mainly due to the of loss of active Li^+: previous studies have well explained that after loss of active Li^+ within layered oxide cathode materials, due to the competing effects of enhanced transitional metal-oxygen attraction and decreased electrostatic repulsion interaction between oxygens, the lattice parameter *c* typically experience a first increase trend.[43] From both the charge/discharge capacities shown from these NMC811||Li half cells and the XRD results, it is concluded that the crystal structure of these cycled NMC811 electrodes are well maintained.

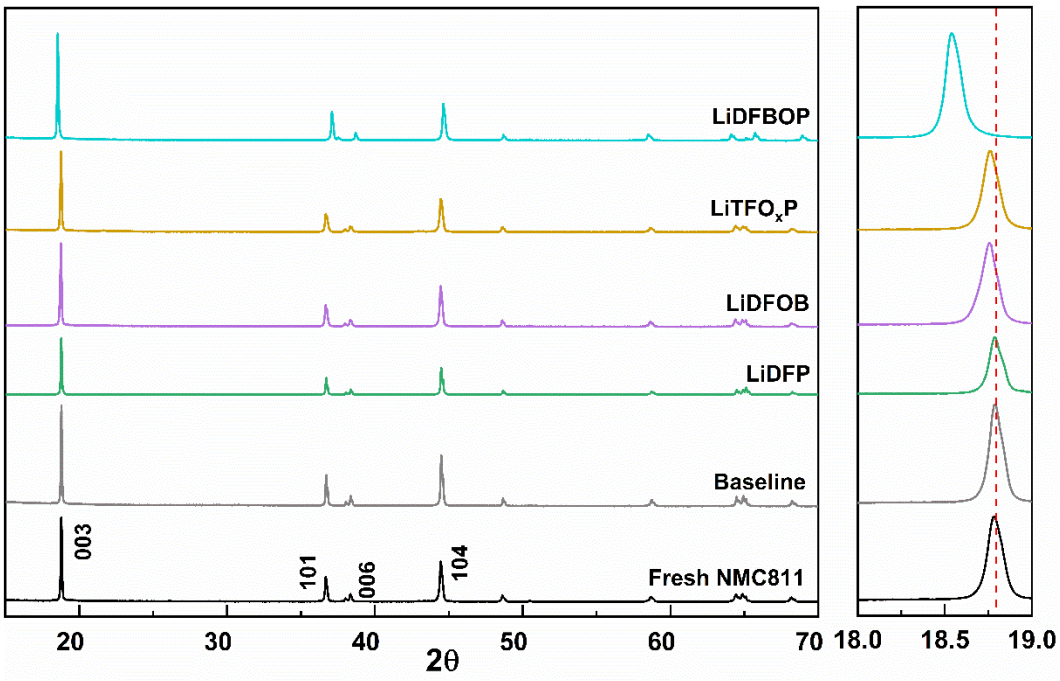

Figure 4. The XRD results for all tested NMC811 cathodes. The cathodes (except the fresh NMC811 cathode) used for the XRD experiments are disassembled from NMC811||Si full cells experiencing 300 cycles at C/3.

Evolution of morphology for electrodes via SEM: For the NMC811 electrodes, the morphologies after the formation process and 300 cycles are summarized respectively in **Figures S9a and S9b**. It is evident that there is no noticeable difference in the evolution of the NMC811 electrodes across the seven samples. This observation is consistent with the structural evolution seen after long-term cycling.

For the Si anodes, optical images shown in **Figure S10** reveal that the baseline and the LiDFP samples exhibit much more severe delamination between the Si electrodes and Cu current collectors compared to the other three electrolytes. This delamination likely contributes to the rapid capacity degradation of the NMC811||Si full cells using these specific electrolytes. Cross-sectional SEM images of the Si anodes were also obtained to examine the evolution of their morphology in the thickness direction, and the results are displayed in **Figure 5** and **Figure S11**. Compared to the pristine Si anode, all Si anodes experience a significant increase in thickness after the formation process: initially, the Si anode is thinner than the Cu current collector, but after formation, its thickness becomes comparable to that of the Cu collector. After 300 cycles, all Si electrodes exhibit a thickness greater than 30 μm. This increase is attributed to the substantial volume expansion of Si electrodes upon alloying with Li^+, as Si typically undergoes a volume expansion of about 300%.[44] Additionally, the evolution of the thickness of Si anodes using different liquid electrolytes was compared. Notably, all additive-containing cells exhibited significantly greater depth of charge and discharge in their Si anodes compared to the baseline cell, as indicated by their higher average capacity over 300 cycles. Among them, the cell with the LiDFBOP additive not only achieved the highest average capacity but also showed the smallest change in electrode thickness after 300 cycles, highlighting the effectiveness of LiDFBOP in stabilizing the Si–electrolyte interphase.

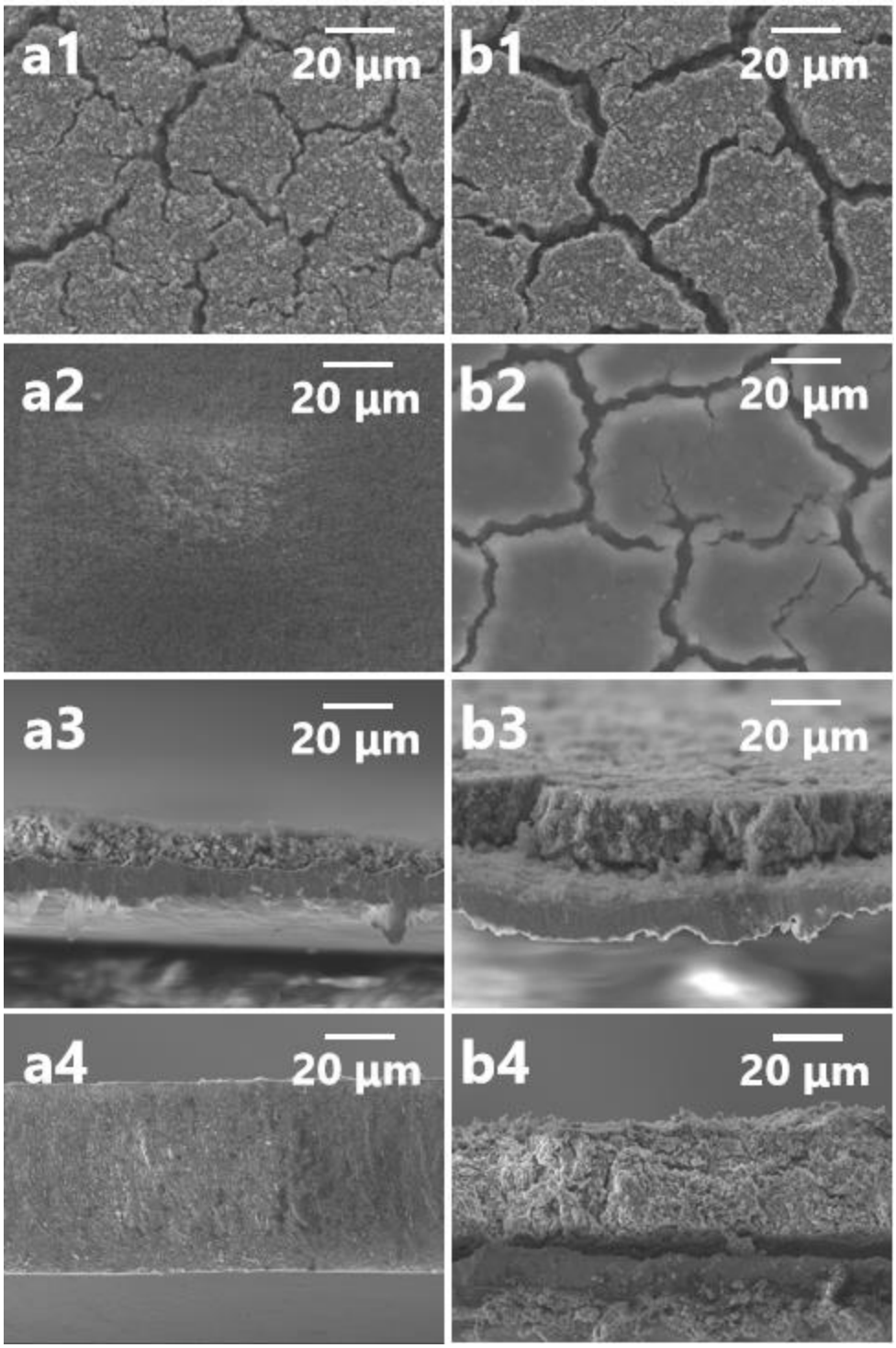

Figure 5. The evolution of morphology for Si electrodes after formation and long-term cycling: a1-b1 morphology of surfaces of Si electrodes experiencing the formation process from Baseline (a1), LiDFBOP (b1); a2-b2 morphology of surfaces of Si electrodes experiencing the long-term cycling; a3-b3 morphology of cross sections of Si electrodes experiencing the formation process; a4-b4 morphology of cross sections of Si electrodes experiencing the long-term cycling. All scale bars in these images represent 20 µm.

Analysis of Interfacial Chemistry via XPS: It is well known that electrolyte/electrode interphases, especially SEIs play a vital role in determining the overall electrochemical performance for LIBs, and our study on solvation structure, bulk crystal structure of NMC811 cathode have well excluded their roles in resulting into the significantly different long-term cycling performances. Thus, we further probed the interphases formed on both NMC811 cathodes and Si anodes via XPS. The full XPS spectra of NMC811 and Si electrodes experiencing the formation process were depicted in **Figure S12**.

Meanwhile, as shown in **Figure 6**, the C 1s and F 1s spectra obtained from NMC811 and Si electrodes are displayed. For the deconvolution of each XPS spectra, peak assignments are based on our previous work. For the C 1s spectra shown in **Figure 6a** and **6c**, it typically deconvolutes into C-C from conductive carbon (~284.8 eV), C-F_2 from PVDF binder (~292 eV) and other carbon-containing products from the decomposition of organic electrolytes. The C 1s spectra of NMC811 cathodes are virtually identical, suggesting all NMC811 show very similar compositions for the interphase formed on NMC811. For the F 1s spectra illustrated in **Figure 6b**, they mainly consisted of CF_2 from the PVDF binder, the $Li_xPO_yF_z$ and LiF from decomposition of $LiPF_6$ salt.[45-48] From the deconvolution results of the F 1s spectra, the 5 samples also showed very similar contents of CF_2, (~688 eV) $Li_xPO_yF_z$ (~687 eV) and LiF (~685 eV). Given the similar chemical compositions and similar contents, it is concluded that the interfacial chemistry at the NMC811 cathode side is not the major player leading to the various performance of tested electrolyte systems.

The interfacial chemistry of the SEI formed on Si anodes was investigated using XPS, with the corresponding spectra shown in **Figure S13**. The C 1s and F 1s spectra are presented in **Figures 6c** and **6d**, respectively. The C 1s spectra from Si anodes, similar to those from NMC811 cathodes, exhibit characteristic peaks: a C–C peak at ~284.8 eV, a C–OR peak at ~287 eV, a C=O peak at ~289 eV, and a Li_2CO_3 peak at ~290 eV. The C 1s spectrum from the baseline Si anode displays a notably high Li_2CO_3 content, whereas the Li_2CO_3 signal is significantly reduced in cells using the other four additives, indicating substantial differences in SEI composition. Notably, the LiDFOB sample shows a higher C=O

content, while the C 1s spectra of all lithium phosphate samples appear similar, suggesting comparable organic SEI compositions. In the F 1s spectra, both LiDFOB and LiDFBOP samples show relatively low levels of LixPOyFz compared to the other three samples, implying a higher LiF content in their SEIs. Overall, the chemical composition analysis of the Si anodes supports our hypothesis that the SEI formed by the LiDFBOP additive exhibits characteristics of LiDFP, LiDFOB, and LiTFOxP, likely due to the dual oxalate rings present in the lithium phosphate salt.

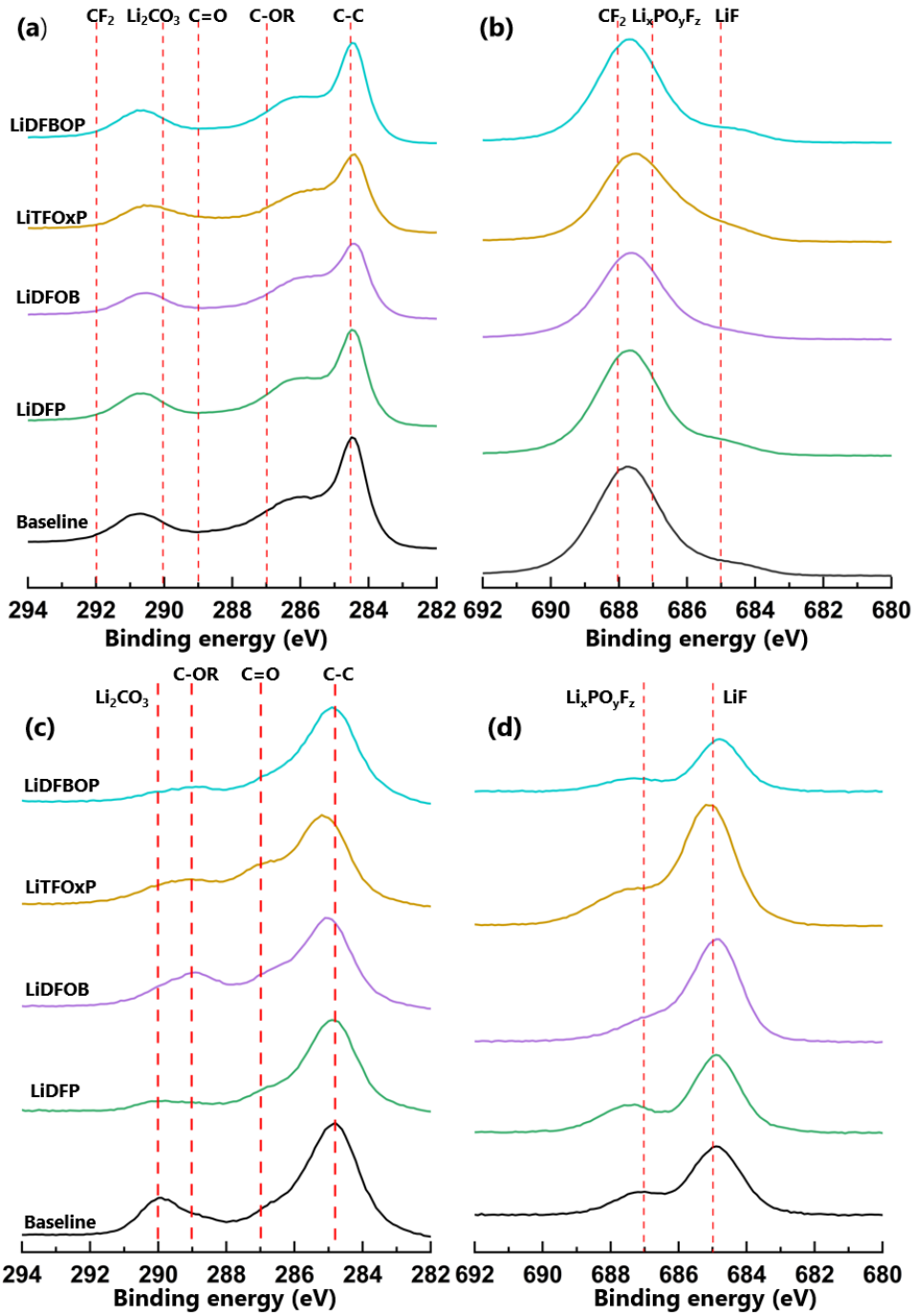

Figure 6. The XPS results for all tested NMC811 cathodes and Si anodes after the formation process: (a) the C 1s spectra of NMC811 cathodes; (b) the F 1s spectra of NMC811 cathodes; (c) the C 1s spectra of Si anodes; (d) the F 1s spectra of Si anodes.

Conclusion

The development of high-performance Si-based lithium-ion batteries requires effective strategies to mitigate challenges such as volume expansion and unstable SEI formation. In this work, six functional additives—VC, VEC, LiDFP, LiDFOB, LiTFOxP, and LiDFBOP—were systematically evaluated in NMC811||Si full cells. Among them, LiDFBOP, a lithium phosphate salt containing dual oxalate groups, exhibited the best electrochemical performance, delivering the highest capacity retention, average specific capacity, and Coulombic efficiency after 300 cycles. Detailed characterization using FTIR, SEM, and XPS revealed that LiDFBOP forms a robust and stable SEI on the Si anode, effectively suppressing continuous side reactions and mitigating electrode pulverization. This superior performance is attributed to the molecular structure of LiDFBOP, which integrates beneficial features of other additives—such as the SEI-forming capabilities of oxalate and phosphate functional groups—into a single compound. Post-cycling analyses confirmed that the NMC811 cathode maintained its structural integrity across all tested electrolytes, and the major differences in cycling performance stem from the interfacial chemistry on the Si anode side. The results of this study highlight the potential of rational additive design to enable durable and high-capacity Si anodes and point toward LiDFBOP as a highly promising candidate for next-generation LIB electrolytes.

KEYWORDS

Lithium-ion batteries, silicon anode, functional additives, solid electrolyte interphase, cyclic oxalate additives

ASSOCIATED CONTENT

Supporting Information

Extra electrochemical data, ^{19}F and ^{31}P NMR spectra for pure LiDFBOP, FTIR data, SEM data,

and XPS data. This material is available free of charge via the Internet.

AUTHOR INFORMATION

Corresponding Author

*Email: csu@anl.gov and amine@anl.gov

Notes

The authors declare no competing financial interest.

ACKNOWLEDGMENTS

This work was conducted as part of the U.S.-German joint collaboration on "Interfaces and Interphases In Rechargeable Li-metal Based Batteries" supported by the U.S. Department of Energy (DOE) and the German Federal Ministry of Education and Research (BMBF). Financial support was provided by the U.S. Department of Energy (DOE), Vehicle Technologies Office (VTO). Argonne National Laboratory is operated for the DOE Office of Science by UChicago Argonne, LLC, under contract number DE-AC02-06CH11357 under the U.S.-Germany Cooperation on Energy Storage. The NMC and Si electrodes were manufactured at the DOE's CAMP Facility, at Argonne National Laboratory. The CAMP Facility is fully supported by the DOE VTO within the core funding of the Applied Battery Research for Transportation Program.

Reference:

1. Nishi, Y., Lithium ion secondary batteries; past 10 years and the future. *Journal of Power Sources* **2001,** *100* (1), 101-106.
2. Asenbauer, J.; Eisenmann, T.; Kuenzel, M.; Kazzazi, A.; Chen, Z.; Bresser, D., The success story of graphite as a lithium-ion anode material – fundamentals, remaining challenges, and recent developments including silicon (oxide) composites. *Sustainable Energy & Fuels* **2020,** *4* (11), 5387-5416.

3. Feyzi, E.; M R, A. K.; Li, X.; Deng, S.; Nanda, J.; Zaghib, K., A comprehensive review of silicon anodes for high-energy lithium-ion batteries: Challenges, latest developments, and perspectives. *Next Energy* **2024,** *5*, 100176.
4. Pollak, E.; Salitra, G.; Baranchugov, V.; Aurbach, D., In Situ Conductivity, Impedance Spectroscopy, and Ex Situ Raman Spectra of Amorphous Silicon during the Insertion/Extraction of Lithium. *The Journal of Physical Chemistry C* **2007,** *111* (30), 11437-11444.
5. Kulova, T. L.; Skundin, A. M.; Pleskov, Y. V.; Terukov, E. I.; Kon'kov, O. I., Lithium insertion into amorphous silicon thin-film electrodes. *Journal of Electroanalytical Chemistry* **2007,** *600* (1), 217-225.
6. Ryu, J.; Hong, D.; Lee, H.-W.; Park, S., Practical considerations of Si-based anodes for lithium-ion battery applications. *Nano Research* **2017,** *10* (12), 3970-4002.
7. Li, H.; Yamaguchi, T.; Matsumoto, S.; Hoshikawa, H.; Kumagai, T.; Okamoto, N. L.; Ichitsubo, T., Circumventing huge volume strain in alloy anodes of lithium batteries. *Nature Communications* **2020,** *11* (1), 1584.
8. Guo, K.; Kumar, R.; Xiao, X.; Sheldon, B. W.; Gao, H., Failure progression in the solid electrolyte interphase (SEI) on silicon electrodes. *Nano Energy* **2020,** *68*, 104257.
9. von Kolzenberg, L.; Latz, A.; Horstmann, B., Chemo-Mechanical Model of SEI Growth on Silicon Electrode Particles. *Batteries & Supercaps* **2022,** *5* (2), e202100216.
10. Yoon, I.; Jurng, S.; Abraham, D. P.; Lucht, B. L.; Guduru, P. R., Measurement of mechanical and fracture properties of solid electrolyte interphase on lithium metal anodes in lithium ion batteries. *Energy Storage Materials* **2020,** *25*, 296-304.
11. Hu, Z.; Zhao, R.; Yang, J.; Wu, C.; Bai, Y., Binders for Si based electrodes: Current status, modification strategies and perspective. *Energy Storage Materials* **2023,** *59*, 102776.
12. Zhang, J.; Zhai, Y.; Zhao, Z.; He, J.; Wei, W.; Xiao, J.; Wu, S.; Yang, Q.-H., Research Progress of Functional Binders in Silicon-Based Anodes for Lithium-Ion Batteries. *Acta Physico-Chimica Sinica* **2024,** *40* (6), 2306006.
13. Eshetu, G. G.; Figgemeier, E., Confronting the Challenges of Next-Generation Silicon Anode-Based Lithium-Ion Batteries: Role of Designer Electrolyte Additives and Polymeric Binders. *ChemSusChem* **2019,** *12* (12), 2515-2539.
14. Zhu, W.; Zhou, J.; Xiang, S.; Bian, X.; Yin, J.; Jiang, J.; Yang, L., Progress of Binder Structures in Silicon-Based Anodes for Advanced Lithium-Ion Batteries: A Mini Review. *Frontiers in Chemistry* **2021,** *Volume 9 - 2021*.
15. Xu, Z.; Yang, J.; Li, H.; Nuli, Y.; Wang, J., Electrolytes for advanced lithium ion batteries using silicon-based anodes. *Journal of Materials Chemistry A* **2019,** *7* (16), 9432-9446.
16. Malkowski, T. F.; Yang, Z.; Sacci, R. L.; Trask, S. E.; Rodrigues, M.-T. F.; Bloom, I. D.; Veith, G. M., Evaluating the roles of electrolyte components on the passivation of silicon anodes. *Journal of Power Sources* **2022,** *523*, 231021.
17. Rajagopalan, B.; Pichardo, M.; de Meatza, I.; Profatilova, I.; Osa, U.; Sananes-Israel, S.; Paillard, E., An ethylene carbonate/propylene carbonate electrolyte for improved cycle life and safety of silicon-graphite/NMC (Ni = 80–83 %) high-energy lithium-ion battery cells. *Journal of Power Sources* **2025,** *627*, 235778.
18. Guo, J.; Omar, A.; Urbanski, A.; Oswald, S.; Uhlmann, P.; Giebeler, L., Electrochemical Behavior of Microparticulate Silicon Anodes in Ether-Based Electrolytes: Why Does LiNO3 Affect Negatively? *ACS Applied Energy Materials* **2019,** *2* (6), 4411-4420.
19. He, S.; Huang, S.; Liu, X.; Zeng, X.; Chen, H.; Zhao, L.; Noor, H.; Hou, X., Electrolyte design for robust gradient solid-electrolyte interfaces to enable high-performance silicon anodes for pouch batteries. *Chemical Engineering Journal* **2024,** *489*, 150620.
20. Johnson, N. M.; Yang, Z.; Kim, M.; Yoo, D.-J.; Liu, Q.; Zhang, Z., Enabling Silicon Anodes with Novel Isosorbide-Based Electrolytes. *ACS Energy Letters* **2022,** *7* (2), 897-905.
21. Wang, S.; Shi, J.; Liu, Z.; Xia, Y., Advanced Ether-Based Electrolytes for Lithium-ion Batteries. *Advanced Energy Materials* **2024,** *14* (37), 2401526.

22. Tong, B.; Song, Z.; Wan, H.; Feng, W.; Armand, M.; Liu, J.; Zhang, H.; Zhou, Z., Sulfur-containing compounds as electrolyte additives for lithium-ion batteries. *InfoMat* **2021,** *3* (12), 1364-1392.
23. Dato, M. A.; Edgington, J.; Hung, C.; Sinha, R.; Liu, Z.; Lopez, J.; Guo, J.; He, M.; Su, C.-C., Sulfur Solutions: Advancing High Voltage and High Energy Lithium Batteries with Organosulfur Electrolytes. *Advanced Energy Materials* **2024,** *14* (13), 2303794.
24. Park, S.; Kim, S.; Lee, J.-A.; Ue, M.; Choi, N.-S., Liquid electrolyte chemistries for solid electrolyte interphase construction on silicon and lithium-metal anodes. *Chemical Science* **2023,** *14* (37), 9996-10024.
25. Wang, F.; Li, P.; Li, W.; Wang, D., Electrochemical Synthesis of Multidimensional Nanostructured Silicon as a Negative Electrode Material for Lithium-Ion Battery. *ACS Nano* **2022,** *16* (5), 7689-7700.
26. Shen, T.; Yao, Z.; Xia, X.; Wang, X.; Gu, C.; Tu, J., Rationally Designed Silicon Nanostructures as Anode Material for Lithium-Ion Batteries. *Advanced Engineering Materials* **2018,** *20* (1), 1700591.
27. Li, P.; Hwang, J.-Y.; Sun, Y.-K., Nano/Microstructured Silicon–Graphite Composite Anode for High-Energy-Density Li-Ion Battery. *ACS Nano* **2019,** *13* (2), 2624-2633.
28. Jia, H.; Zheng, J.; Song, J.; Luo, L.; Yi, R.; Estevez, L.; Zhao, W.; Patel, R.; Li, X.; Zhang, J.-G., A novel approach to synthesize micrometer-sized porous silicon as a high performance anode for lithium-ion batteries. *Nano Energy* **2018,** *50*, 589-597.
29. Jia, H.; Li, X.; Song, J.; Zhang, X.; Luo, L.; He, Y.; Li, B.; Cai, Y.; Hu, S.; Xiao, X.; Wang, C.; Rosso, K. M.; Yi, R.; Patel, R.; Zhang, J.-G., Hierarchical porous silicon structures with extraordinary mechanical strength as high-performance lithium-ion battery anodes. *Nature Communications* **2020,** *11* (1), 1474.
30. Zhang, S. S., A review on electrolyte additives for lithium-ion batteries. *Journal of Power Sources* **2006,** *162* (2), 1379-1394.
31. Qian, Y.; Hu, S.; Zou, X.; Deng, Z.; Xu, Y.; Cao, Z.; Kang, Y.; Deng, Y.; Shi, Q.; Xu, K.; Deng, Y., How electrolyte additives work in Li-ion batteries. *Energy Storage Materials* **2019,** *20*, 208-215.
32. Ming, J.; Cao, Z.; Wu, Y.; Wahyudi, W.; Wang, W.; Guo, X.; Cavallo, L.; Hwang, J.-Y.; Shamim, A.; Li, L.-J.; Sun, Y.-K.; Alshareef, H. N., New Insight on the Role of Electrolyte Additives in Rechargeable Lithium Ion Batteries. *ACS Energy Letters* **2019,** *4* (11), 2613-2622.
33. Zhang, S. S., Design aspects of electrolytes for fast charge of Li-ion batteries. *InfoMat* **2021,** *3* (1), 125-130.
34. K, B.; Jareer, M.; Lakshmi Sagar, G.; Mukesh, P.; A, A.; Mandal, D.; Nagaraja, H. S.; Shahgaldi, S., Advanced Electrolyte Additives for Lithium-Ion Batteries: Classification, Function, and Future Directions. *The Journal of Physical Chemistry C* **2025,** *129* (25), 11221-11251.
35. Zhang, H.; Eshetu, G. G.; Judez, X.; Li, C.; Rodriguez-Martínez, L. M.; Armand, M., Electrolyte Additives for Lithium Metal Anodes and Rechargeable Lithium Metal Batteries: Progress and Perspectives. *Angewandte Chemie International Edition* **2018,** *57* (46), 15002-15027.
36. Nam, J.; Lee, H.; Chae, O. B. *Overcoming Challenges in Silicon Anodes: The Role of Electrolyte Additives and Solid-State Electrolytes. Micromachines* **2025**, *16*, 800.
37. Kondracki, Ł.; Kalita, M.; Zhang, X.; Müller, K.; Kowalczyk, P.; Majchrzak, P.; et al. *Synergy of Artificial SEI and Electrolyte Additive for Improved Performance of Silicon Electrodes in Li-Ion Batteries. ACS Appl. Energy Mater.* **2024**, *7*(20), 9336–9348.
38. Choi, N.-S.; Yew, K. H.; Lee, K. Y.; Sung, M.; Kim, H.; Kim, S.-S., Effect of fluoroethylene carbonate additive on interfacial properties of silicon thin-film electrode. *Journal of Power Sources* **2006,** *161* (2), 1254-1259.
39. Chen, L.; Wang, K.; Xie, X.; Xie, J., Effect of vinylene carbonate (VC) as electrolyte additive on electrochemical performance of Si film anode for lithium ion batteries. *Journal of Power Sources* **2007,** *174* (2), 538-543.

40. Zhang, F.; Yang, J., Boosting initial coulombic efficiency of Si-based anodes: a review. *Emergent Materials* **2020,** *3* (3), 369-380.
41. Sun, L.; Liu, Y.; Wu, J.; Shao, R.; Jiang, R.; Tie, Z.; Jin, Z., A Review on Recent Advances for Boosting Initial Coulombic Efficiency of Silicon Anodic Lithium Ion batteries. *Small* **2022,** *18* (5), 2102894.
42. Kim, M.; Yang, Z.; Son, S.-B.; Trask, S. E.; Jansen, A.; Bloom, I., Effect of cathode on crosstalk in Si-based lithium-ion cells. *Journal of Materials Chemistry A* **2021,** *9* (47), 26904-26916.
43. Liu, J.; Du, Z.; Wang, X.; Tan, S.; Wu, X.; Geng, L.; Song, B.; Chien, P.-H.; Everett, S. M.; Hu, E., Anionic redox induced anomalous structural transition in Ni-rich cathodes. *Energy & Environmental Science* **2021,** *14* (12), 6441-6454.
44. Moyassari, E.; Roth, T.; Kücher, S.; Chang, C.-C.; Hou, S.-C.; Spingler, F. B.; Jossen, A., The Role of Silicon in Silicon-Graphite Composite Electrodes Regarding Specific Capacity, Cycle Stability, and Expansion. *Journal of The Electrochemical Society* **2022,** *169* (1), 010504.
45. Philippe, B.; Dedryvère, R.; Allouche, J.; Lindgren, F.; Gorgoi, M.; Rensmo, H.; Gonbeau, D.; Edström, K., Nanosilicon Electrodes for Lithium-Ion Batteries: Interfacial Mechanisms Studied by Hard and Soft X-ray Photoelectron Spectroscopy. *Chemistry of Materials* **2012,** *24* (6), 1107-1115.
46. Philippe, B.; Dedryvère, R.; Gorgoi, M.; Rensmo, H.; Gonbeau, D.; Edström, K., Improved Performances of Nanosilicon Electrodes Using the Salt LiFSI: A Photoelectron Spectroscopy Study. *Journal of the American Chemical Society* **2013,** *135* (26), 9829-9842.
47. Jeschull, F.; Lindgren, F.; Lacey, M. J.; Björefors, F.; Edström, K.; Brandell, D., Influence of inactive electrode components on degradation phenomena in nano-Si electrodes for Li-ion batteries. *Journal of Power Sources* **2016,** *325*, 513-524.
48. Yu, W.; Yu, Z.; Cui, Y.; Bao, Z., Degradation and Speciation of Li Salts during XPS Analysis for Battery Research. *ACS Energy Letters* **2022,** *7* (10), 3270-3275.